Journal of Solid State Chemistry 183 (2010) 1847–1852

Contents lists available at ScienceDirect

Journal of Solid State Chemistry

journal homepage: www.elsevier.com/locate/jssc

Eu^{3+} luminescence in $La_5Si_2BO_{13}$ with apatite related structure and magnetic studies in $Ln_5Si_2BO_{13}$ (Ln=Gd, Dy)

S. Asiri Naidu [a], U.V. Varadaraju [a,*], B. Raveau [b]

[a] Materials Science Research Centre, Indian Institute of Technology Madras, Chennai 600036, India
[b] Laboratoire de Crystallographie et Sciences des Matériaux, ENSICAEN, UniVersité de Caen, CNRS, 6 Bd Maréchal Juin, F-14050 Caen 4, France

ARTICLE INFO

Article history:
Received 7 March 2010
Received in revised form
26 May 2010
Accepted 29 May 2010
Available online 8 June 2010

Keywords:
Photoluminescence
Apatite
X-ray diffraction
Eu^{3+} as a structure probe

ABSTRACT

Eu^{3+} photoluminescence is studied in $La_5Si_2BO_{13}$ with apatite related structure. $La_{5-x}Eu_xSi_2BO_{13}$ [x=0.05, 0.1, 0.3, 0.5, 0.7, 1.0, 2.0] compositions are synthesized. The emission results shows that Eu^{3+} ions occupy two different cationic sites viz., La(1) and La(2). The increase in the intensity of $^5D_0$–$^7F_0$ line with increasing Eu^{3+} content shows the preferential occupancy of Eu^{3+} in La(2) site due to the existence of short La(2)–O(4) (free oxide ion) bond. The observation of antiferromagnetic interactions in Gd and Dy analogues supports the structural features elucidates from photoluminescence studies.

1. Introduction

Apatites have the general formula $A_5(TO_4)_3X$ in which A stands for the alkali, alkaline earth, trivalent rare earth ions, Pb and Cd metals, T for P, As, Sb, V, Mn, Cr, Si, and Ge and X for F^-, Cl^-, O^{2-}, S^{2-}, OH^- and CO_3^{2-}. The representative of the apatite family is $Ca_5(PO_4)_3F$. It crystallizes in the space group $P6_3/m$ [1] and has two sites for cations viz., a nine-coordinated 4*f* site (C_3 symmetry) and a seven-coordinated 6*h* site (C_s symmetry). In oxyapatites (X=Oxygen), the O(4) ion (free oxide ion) does not belong to any tetrahedron. It is coordinated only to three cations present in the 6*h* site. Thus, electrostatic interactions between the O(4) ion and the cations are inadequate. As a result, the 6*h* site has more covalent nature than 4*f* site. Thus, cations with low charge and large radius will not occupy the 6*h* site. Indeed, the 4*f* sites are either vacant or are occupied by A^+ and A^{2+} ions. Cations with high charge (A^{3+}) preferentially occupy 6*h* sites. The distribution of the A^{3+} cations between the 4*f* and 6*h* sites depends on the size and ionicity of the A^{3+} ion [2]. The free oxide ion (O(4)) is situated in the plane of the triangle formed by three *A*—cations. Apatite structure is versatile. By an appropriate choice of anions and cations, several isostructural compounds can be synthesized.

Apatites are known to be good host lattices for many luminescent centers [3,4]. The mineral, $Ca_{10}(PO_4)_6(F,Cl)_2$, with apatite structure, doped with Mn^{2+} and Sb^{3+} is a well-known phosphor for fluorescent lamps [5]. Eu^{3+}, being the most important emitter in the red region of the visible spectrum, has been utilized extensively in color televisions and high efficiency fluorescent lamps [6]. Eu^{3+} has a simple electronic energy level scheme among the rare earth ions and the transitions are hypersensitive, i.e., they depend strongly on the chemical surroundings [7]. Because of these hypersensitive transitions, Eu^{3+} has been used as a local structure probe in determining the microscopic symmetries of different sites available in various host lattices, such as apatites [8–10]. Such studies are important to understand physical properties. For example, recently, the rare earth containing silicate and germinates oxyapatites have drawn considerable attention due to their high oxide ion conductivity [11,12]. Understanding the cation distribution in the lattice would help in shedding light on the ionic conduction mechanism in these lattices.

$La_5Si_2BO_{13}$ crystallizes with apatite related structure [13]. The crystal structure of $La_5Si_2BO_{13}$ is shown in Fig. 1. Eu^{3+} luminescence has been reported in $La_5Si_2BO_{13}$:2%Eu and the results suggested that Eu^{3+} occupies two different crystallographic sites [14]. In the present study, Eu^{3+} luminescence is used as a local structural probe to ascertain the above observation and to understand the site occupancy behavior as a function of Eu^{3+} concentration in $La_5Si_2BO_{13}$ host lattice. In addition, the Gd and Dy analogues of $La_5Si_2BO_{13}$ have been synthesized and the magnetic properties have been investigated.

2. Experimental

2.1. Synthesis

$La_{5-x}Eu_xSi_2BO_{13}$ [x=0.05, 0.1, 0.3, 0.5, 0.7, 1.0, 2.0] and $Ln_5Si_2BO_{13}$ (Ln=Pr, Nd, Sm, Eu, Gd, Dy) phases were synthesized

* Corresponding author.
E-mail address: varada@iitm.ac.in (U.V. Varadaraju).

0022-4596/$ - see front matter © 2010 Published by Elsevier Inc.
doi:10.1016/j.jssc.2010.05.034

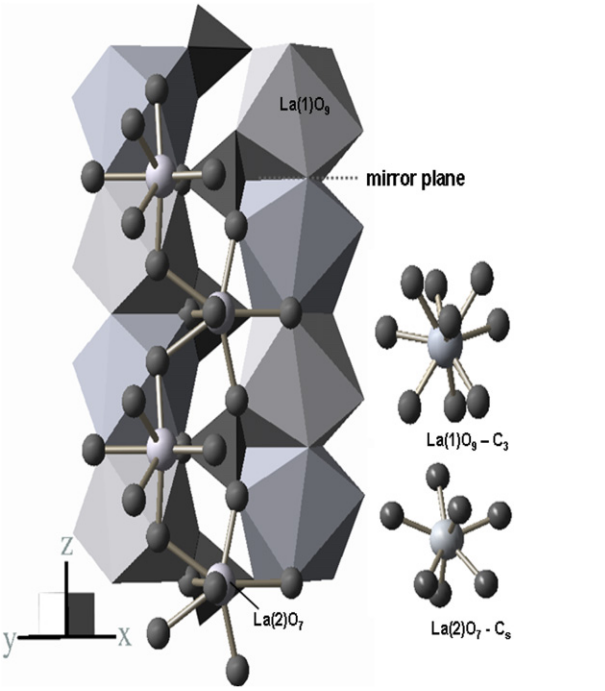

Fig. 1. Crystal structure of $La_5Si_2BO_{13}$.

by the conventional high temperature solid state reaction method. Ln_2O_3 (Ln=La, Pr, Nd, Sm, Eu, Gd, Dy) were preheated at 1100 °C overnight. The reactants were Ln_2O_3 (Ln=La, Pr, Nd, Sm, Eu, Gd, Dy, Indian Rare Earths, 99.9%), H_3BO_3 (Merck, 99.8%), SiO_2 (Thermal Syndicate, 99.9%). Typically, the reactants were mixed in stoichiometric proportions and heated in alumina crucibles at different temperatures with intermittent grindings. The heating conditions employed are 300 °C for 6 h, 700 °C for 12 h, 950 °C for 12 h, 1200 °C for 48 h (for $La_{5-x}Eu_xSi_2BO_{13}$ phases), 900 °C for 24 h, 1400 °C for 24 h and 1500 °C for 12 h for $Ln_5Si_2BO_{13}$ (Ln=Pr, Nd, Sm, Eu, Gd, Dy) phases.

2.2. Characterization

The powder X-ray diffraction (XRD) patterns were recorded on a Philips diffractometer (Cu$K\alpha$ radiation). The diffraction patterns were indexed based on the reported pattern of $La_5Si_2BO_{13}$; hexagonal system, space group $P6_3/m$ (JCPDS file no. 52-0699). The cell parameters were calculated by least square fitting method. Photoluminescence excitation and emission spectra were recorded on powder samples at room temperature using a spectrofluorometer (FP-6500, JASCO). An R-60 glass filter was used while recording the excitation spectra to remove the lower order reflections of the emission wavelength for which the excitation is recorded. Magnetic susceptibility measurements were carried out in the temperature range 4.2–300 K in magnetic fields up to 5 T using a SQUID magnetometer (quantum design).

3. Results and discussion

3.1. Phase formation

Fig. 2 shows powder XRD patterns of $La_{5-x}Eu_xSi_2BO_{13}$ [x=0.05, 0.1, 0.3, 0.5, 0.7, 1.0, 2.0] compositions. The reported XRD pattern of the parent $La_5Si_2BO_{13}$ is given for comparison. It is evident from the XRD patterns that all the compositions have good crystallinity. A small impurity line at 2θ=29° is observed for these series of

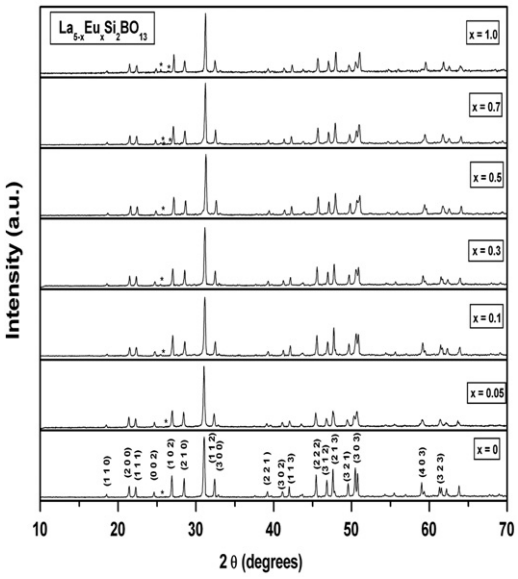

Fig. 2. Powder XRD patterns of $La_{5-x}Eu_xSi_2BO_{13}$ phases.

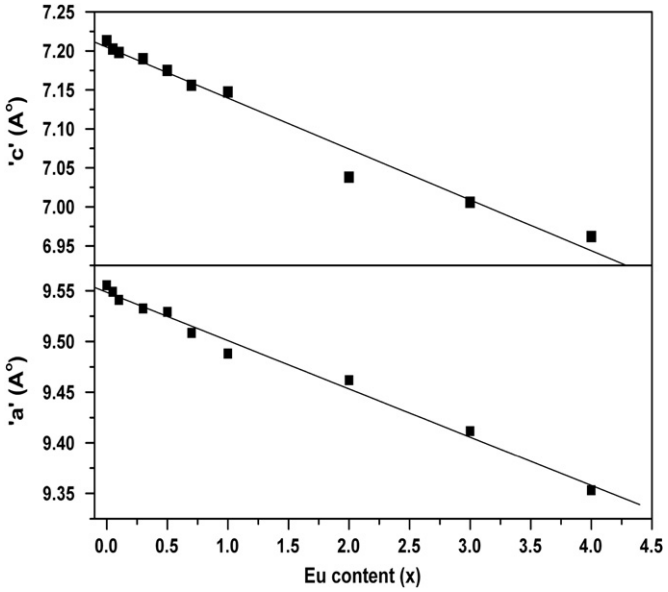

Fig. 3. Variation of hexagonal 'a' and 'c' lattice parameters with Eu^{3+} content in $La_{5-x}Eu_xSi_2BO_{13}$ [x=0, 0.05, 0.1, 0.3, 0.5, 0.7, 1.0, 2.0, 3.0, 4.0].

compounds and this could be identified as $LaBO_3$. All the lines can be indexed based on a hexagonal cell and the synthesized compositions are isostructural with parent $La_5Si_2BO_{13}$ compound. The variation in the hexagonal 'a' and 'c' lattice parameters with Eu content is shown in Fig. 3. Lattice contraction is evident with increasing Eu substitution suggesting solid solution formation. Vegard's law behavior suggests statistical distribution of the substituent in the lattice.

3.2. Diffuse reflectance spectroscopy

The diffuse reflectance spectra (DRS) of $La_5Si_2BO_{13}$ and $La_4EuSi_2BO_{13}$ recorded at room temperature are shown in the inset of Fig. 4. In the case of Eu^{3+} substituted compound the broadband (250–300 nm) is due to the charge transfer from O^{2-}–Eu^{3+}. The sharp absorption lines correspond to the

transitions within the $4f^6$ levels of the trivalent europium. The band gap values derived using the Kubelka–Munk function are 6.31 eV and 6.41 eV for $La_5Si_2BO_{13}$ and $La_4EuSi_2BO_{13}$, respectively. These optical band gap values are smaller than that of silicates and borates for instance RE_2SiO_5 and RBO_3 [15], which could be due to the presence of free oxide ions [O(4)] in apatite structures. The covalent nature of the metal O(4) bond leads to band broadening and thereby results in reduction of band gap.

3.3. Photoluminescence studies

3.3.1. $La_{5-x}Eu_xSi_2BO_{13}$ [x=0.05, 0.1, 0.3, 0.5, 0.7, 1.0, 2.0]

Fig. 4 shows the photoluminescence excitation spectra of Eu^{3+} in $La_5Si_2BO_{13}$ host lattice for different Eu^{3+} concentrations. The spectra are recorded under 617 nm emission. The excitation spectra show a band in the region 230–350 nm with λ_{max}=293 nm and this corresponds to O^{2-}–Eu^{3+} charge transfer band (CTB) and correlates well with DRS data. The CTB maximum value is higher when compared with O^{2-}–Eu^{3+} CTB maximum (270 nm) in $LaBO_3$:Eu^{3+} [16]. The charge transfer transitions depend on covalent nature of O^{2-}–Eu^{3+} bond; the higher the covalency of the O^{2-}–Eu^{3+} bond, the absorption maximum shifts towards longer wavelength side. In the present study, the large shift in CTB maximum reveals the more covalent nature of O^{2-}–Eu^{3+} bond [due to the presence free oxide ion O(4)]. The sharp excitation peaks between 350 and 500 nm correspond to Eu^{3+} intra-4f transitions. The excitation of Eu^{3+} occurs from the ground $^7F_0$ level to various higher levels of Eu^{3+} ion. The $^7F_0$–$^5L_6$ line at 394 nm is the strongest line in the excitation spectra. An interesting observation is that the intensity of CTB transitions is more than that of intra-4f transitions at lower Eu^{3+} concentration ($x \le 0.1$) and at higher Eu^{3+} concentrations ($x \ge 0.1$) the converse is observed. A similar observation is made in the cation and anion-deficient silicate apatite $Sr_3(La_{1-x}Eu_x)(SiO_4)_6$ [17].

The PL emission spectra of $La_{5-x}Eu_xSi_2BO_{13}$ [x=0.05, 0.1, 0.3, 0.5, 0.7, 1.0, 2.0] under 394 and 465 nm excitation wavelengths are shown in Figs. 5 and 6, respectively. A single emission line is

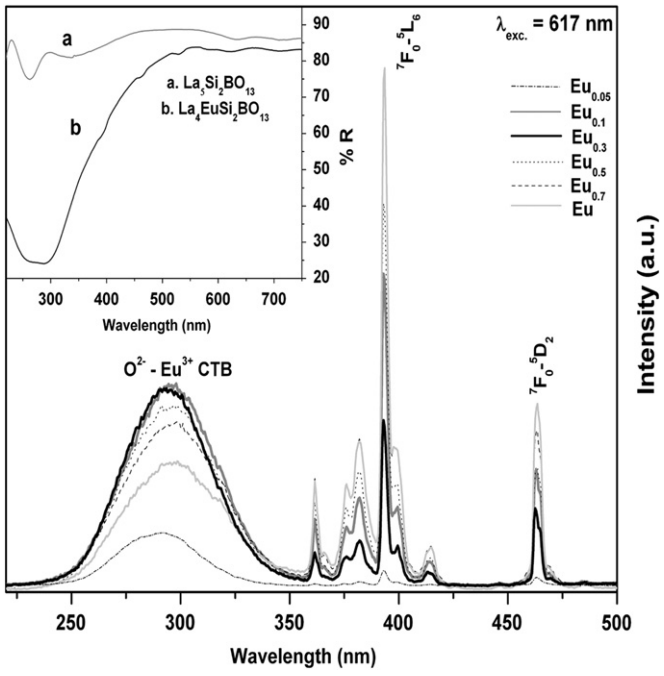

Fig. 4. Photoluminescence excitation spectra of $La_{5-x}Eu_xSi_2BO_{13}$ (x=0.05, 0.1, 0.3, 0.5, 0.7, 1). Inset shows the diffuse reflectance spectra of $La_5Si_2BO_{13}$ and $La_4EuSi_2BO_{13}$.

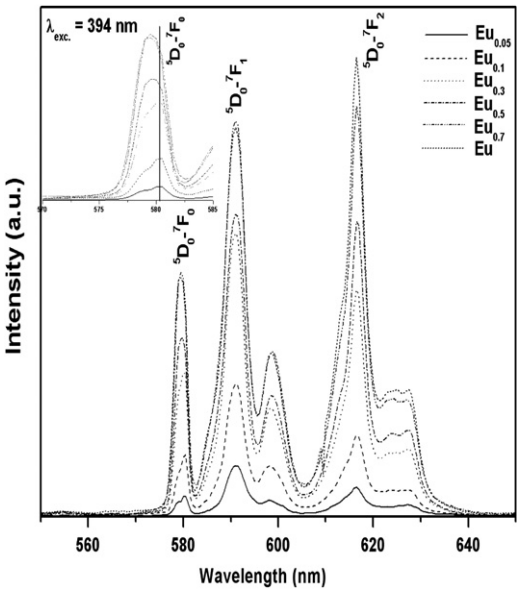

Fig. 5. Emission spectra of $La_{5-x}Eu_xSi_2BO_{13}$ under 394 nm excitation wavelength.

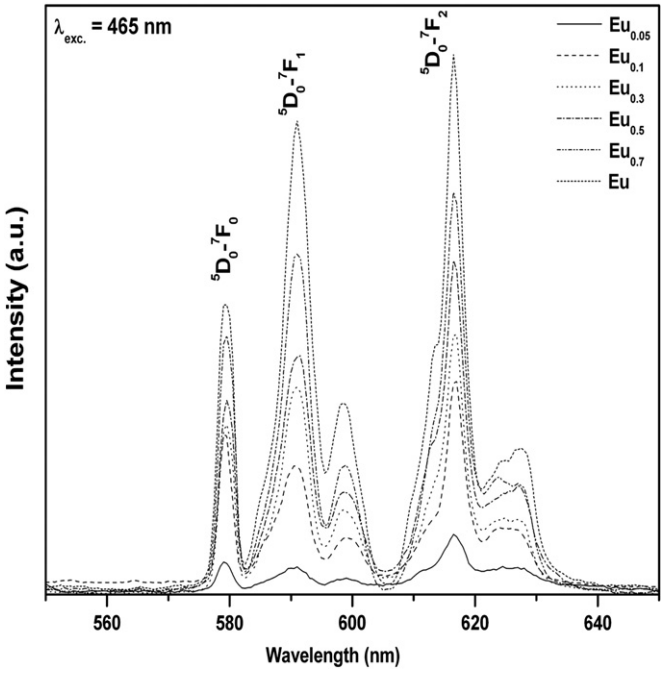

Fig. 6. Emission spectra of $La_{5-x}Eu_xSi_2BO_{13}$ under 465 nm excitation wavelength.

observed at 579 nm and is attributed to $^5D_0$–$^7F_0$ transition which shows small splitting for low concentrations of Eu^{3+} doping ($x \le 0.1$). It is a well-known fact that the $^5D_0$–$^7F_0$ transitions are usually observed when Eu^{3+} occupies a site with either C_n, C_{nv} or C_s symmetry. In the presently studied compound, $La_5Si_2BO_{13}$, the local site symmetry of La(2) (6h site) is C_s and that of La(1) (4f site) is C_3. Thus, from the presence of emission line corresponding to $^5D_0$–$^7F_0$ transition, it can be concluded that Eu^{3+} occupies either of the sites. However, the splitting of the line corresponding to the $^5D_0$–$^7F_0$ transition indicates the presence of Eu^{3+} in more than one crystallographic site. This splitting is very clearly observed at low concentrations of Eu^{3+} and as the concentration increases, these two emission lines overlap with each other resulting in the broadness of $^5D_0$–$^7F_0$ transition as observed in the inset in Fig. 6.

Due to experimental restrictions, we could get only the room temperature data and low temperature data will show this splitting very clearly. The presence of two emission lines for $^5D_0$–$^7F_0$ line even at $x=0.05$ and 0.1 show that Eu^{3+} distributes in the 6*h* as well as 4*f* sites. In general, cations with small size prefer the 6*h* site due to the higher electrostatic charge available due to the presence of free oxygen [2]. Eu^{3+} (0.91 Å) being smaller than La^{3+} (1.01 Å) is expected to occupy the 6*h* site albeit, not small enough to prefer the 6*h* site exclusively. Accordingly, in the present case, it is observed that Eu^{3+} occupies both 6*h* and 4*f* sites.

The important feature is the strong emission intensity of this forbidden transition. It is reported that $^5D_0$–$^7F_0$ transition will have high intensity when there exists a short and highly covalent Eu^{3+}–O^{2-} bond [18]. In $La_5Si_2BO_{13}$, the La(2) site has more covalent nature than La(1) because of existence of short La(2)–O(4) (free oxygen ion) bond. Thus, it is expected that Eu^{3+} preferentially occupies the La(2) site. The intensity of the $^5D_0$–$^7F_0$ transition increases with increase in Eu^{3+} concentration. At low Eu^{3+} concentrations ($x \leq 0.1$), the $^5D_0$–$^7F_0$ emission maximum is at 580.5 nm and a shoulder is clearly observed at 579.5 nm. As the Eu^{3+} concentration increases, the emission maximum of $^5D_0$–$^7F_0$ transition shifts towards 579.5 nm. This points out that more Eu^{3+} occupies either La(1) or La(2) sites predominantly. A similar behavior was reported in the case of $Bi_{1-x}Eu_xCa_4(PO_4)_3O$ where more Eu^{3+} occupies Ca(2) site with an irregular coordination environment at higher concentration and in that case the Bi^{3+} with the $6s^2$ lone pair electrons prevent Eu^{3+} to occupy Ca(2) site at low concentrations [19]. Similarly, in the present study, the shift in the emission maximum of $^5D_0$–$^7F_0$ transition can be assigned to the predominant occupancy of Eu^{3+} in the La(2) site at higher concentrations. Another proof for this arises from the relative emission intensity of magnetic and electric dipole transitions, $^5D_0$–$^7F_1$ and $^5D_0$–$^7F_2$, respectively. An insight into this will provide important information related to the occupancy of Eu^{3+} in different crystallographic sites in the apatite crystal structure. The magnetic-dipole transition $^5D_0$–$^7F_1$ is dominant when Eu^{3+} occupies a site with center of symmetry and in the case of non-centrosymmetric environment the electric dipole transition $^5D_0$–$^7F_2$ will be the intense emission line [7]. A change in the relative emission intensities of these lines with increasing Eu^{3+} content will reveal the change in the Eu^{3+} environment. Under 394 nm excitation wavelength, the $^5D_0$–$^7F_1$ line is higher in intensity than the $^5D_0$–$^7F_2$ line at lower Eu^{3+} concentrations. The intensity of $^5D_0$–$^7F_2$ transition line increases for higher Eu^{3+} concentrations. This clearly points that Eu^{3+} occupies a more symmetric site at low concentrations and this site is the La(1) site with 9 coordination and at high concentrations the irregularly coordinated La(2) site is occupied. In contrast, under 465 nm excitation wavelength, the intensity of $^5D_0$–$^7F_2$ transition line is relatively higher than that of the $^5D_0$–$^7F_1$ transition line at all Eu^{3+} concentrations.

The Eu^{3+} emission spectra of $La_3Eu_2Si_2BO_{13}$ compound under 394 and 465 nm excitations are shown in Fig. 7. From the emission spectra it is clear that the electric dipole $^5D_0$–$^7F_2$ transition is more intense than the magnetic-dipole $^5D_0$–$^7F_1$ transition. It is obvious that Eu^{3+} ions predominantly occupies the La(2) site.

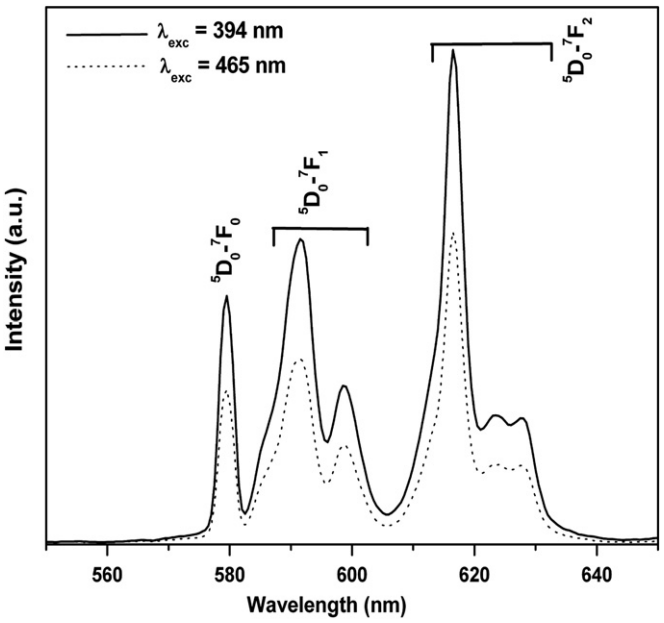

Fig. 7. Emission spectra of $La_3Eu_2Si_2BO_{13}$ under different excitation wavelengths.

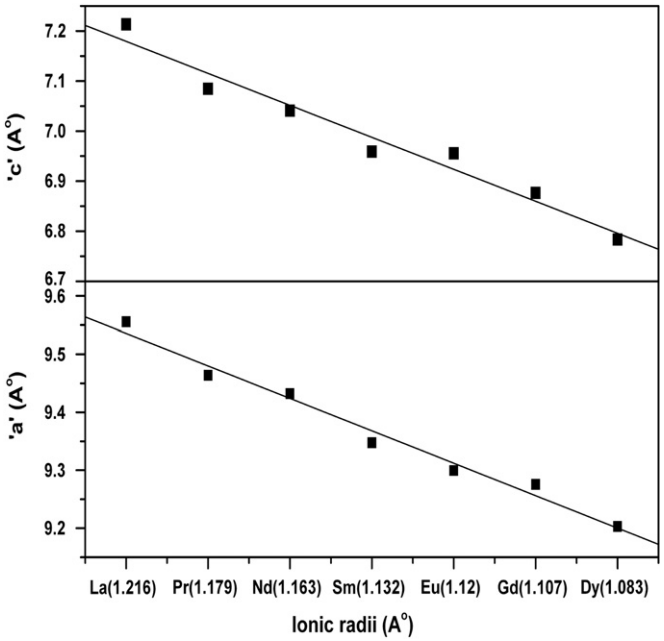

Fig. 8. Variation of hexagonal '*a*' and '*c*' lattice parameters with ionic radii of $Ln_5Si_2BO_{13}$ (*Ln*=La, Pr, Nd, Sm, Eu, Gd, Dy).

3.3.2. $Ln_5Si_2BO_{13}$ (*Ln*=Pr, Nd, Sm, Eu, Gd, Dy)

All the title compounds are synthesized for the first time in the present study. The XRD patterns show that all are single phase suggesting that the apatite structure is flexible enough to accommodate wide ionic size range. The patterns could be indexed based on a hexagonal unit cell with space group $P6_3/m$, isostructural with $La_5Si_2BO_{13}$. The variation in lattice parameters as a function of the ionic radii of the lanthanides is linear (Fig. 8). An intriguing feature is that both the hexagonal '*a*' and '*c*' parameters contract with decreasing size of the lanthanide ion. In apatites with space group $P6_3/m$, substitutions at 6*h* lattice site results in the variation in the '*a*' axis [20]. Substitutions at the 4*f* site do not affect the '*a*' axis since shorter bonds of 6*h* site lie in the directions [h k 0]. It is also reported that the variation in '*c*' lattice parameter depends on the substitutions at the 4*f* site. The crystal structure of $La_5Si_2BO_{13}$ with space group $P6_3/m$ is close to that of apatite. Thus, the observed variation of both '*a*' and '*c*' parameters reveals that indeed the lanthanide ions are distributed on both 6*h* and 4*f* site. This is in agreement with the conclusions drawn regarding the site occupancy of Eu^{3+} from PL studies as reported in the previous sections.

Table 1
Atomic coordinates and agreement factor of $Ln_5Si_2BO_{13}$ [Ln=Gd, Dy].

	$Gd_5Si_2BO_{13}$	$Dy_5Si_2BO_{13}$
4*f*	Gd(1)-0.3333[a] 1/3,2/3,−0.0047(8)	Dy(1)-0.3333[a] 1/3,2/3,−0.0046(7)
6*h*	Gd(2)-0.5[a] 0.2324, −0.0115,1/4	Gd(2)-0.5[a] 0.2336, −0.0091,1/4
6*h*	B-0.1666[a] 0.4036, 0.3741,1/4	B-0.1666[a] 0.4036, 0.3741,1/4
6*h*	Si-0.3333[a] 0.4036,0.3741,1/4	Si-0.3333[a] 0.4036,0.3741,1/4
6*h*	O(1)-0.5[a] 0.3273,0.4848,1/4	O(1)-0.5[a] 0.3273,0.4848,1/4
6*h*	O(2)-0.5[a] 0.5952,0.4683,1/4	O(2)-0.5[a] 0.5952,0.4683,1/4
12*i*	O(3)-1.0[a] 0.3452,0.2559,0.0719	O(3)-1.0[a] 0.3452,0.2559,0.0719
2*a*	O(4)-0.1666[a] 0,0,1/4	O(4)-0.1666[a] 0,0,1/4
R_p	1.69	1.51
R_{wp}	15.7	11.8
R_{exp}	1.31	1.2
χ^2	3.24	2.84

[a] Occupancy.

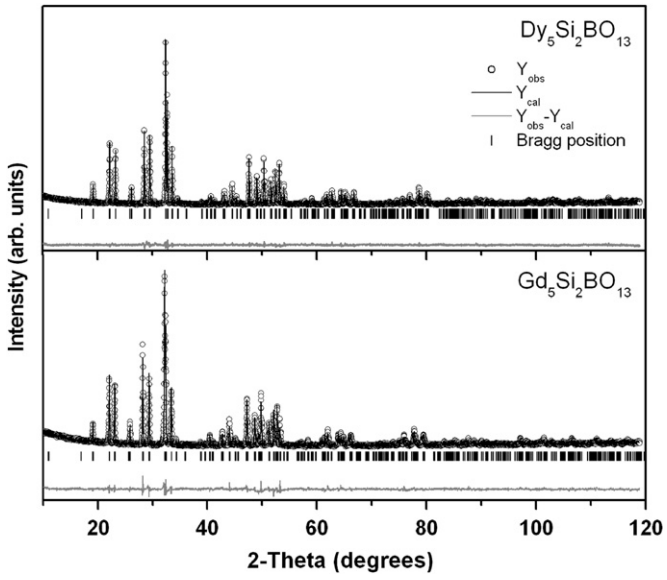

Fig. 9. Observed, calculated and difference powder X-ray diffraction profiles of $Ln_5Si_2BO_{13}$ (Ln=Gd, Dy).

Slow scan XRD data were collected on two representative compounds viz., $Ln_5Si_2BO_{13}$ (Ln=Gd, Dy). The Rietveld refinement of the powder XRD patterns was done using the FULLPROF program starting with a model of $La_5Si_2BO_{13}$ with the space group $P6_3/m$ (n=176). An excellent fit was obtained for these two compounds using the hexagonal $P6_3/m$ symmetry model (Table 1). The observed, calculated, and difference profiles of $Ln_5Si_2BO_{13}$ (Ln=Gd, Dy) compounds are shown in Fig. 9. The difference between the shorter and the longer Ln–O distances is a measure of the index of the polyhedral distortion. Greater the difference, higher is the polyhedral distortion. The difference in La(1)–O(3) and La(1)–O(1) is 0.335 Å reported earlier [13] is higher than the difference in Gd(1)–O(3) and Gd(1)–O(1) (0.3231 Å) and Dy(1)–O(3) and Dy(1)–O(1) (0.3283 Å) from the present study. Thus, the La(1)O_9 polyhedra are highly distorted compared to those of Gd(1)O_9 and Dy(1)O_9 polyhedra.

3.3.3. *Magnetic susceptibility studies on $Ln_5Si_2BO_{13}$ (Ln=Gd, Dy)*

The temperature dependence of the magnetic susceptibilities (χ) for $Ln_5Si_2BO_{13}$ (Ln=Gd, Dy) was measured in the temperature range of 4.2–350 K at two different fields, 50 Oe and 5 T. The 1/chi vs. T plots are presented in Figs. 10 (a) & (b). Insets of Fig. 10 shows the plots of reciprocal magnetic susceptibility versus temperature in the range 4.2–40 K. Deviation from the

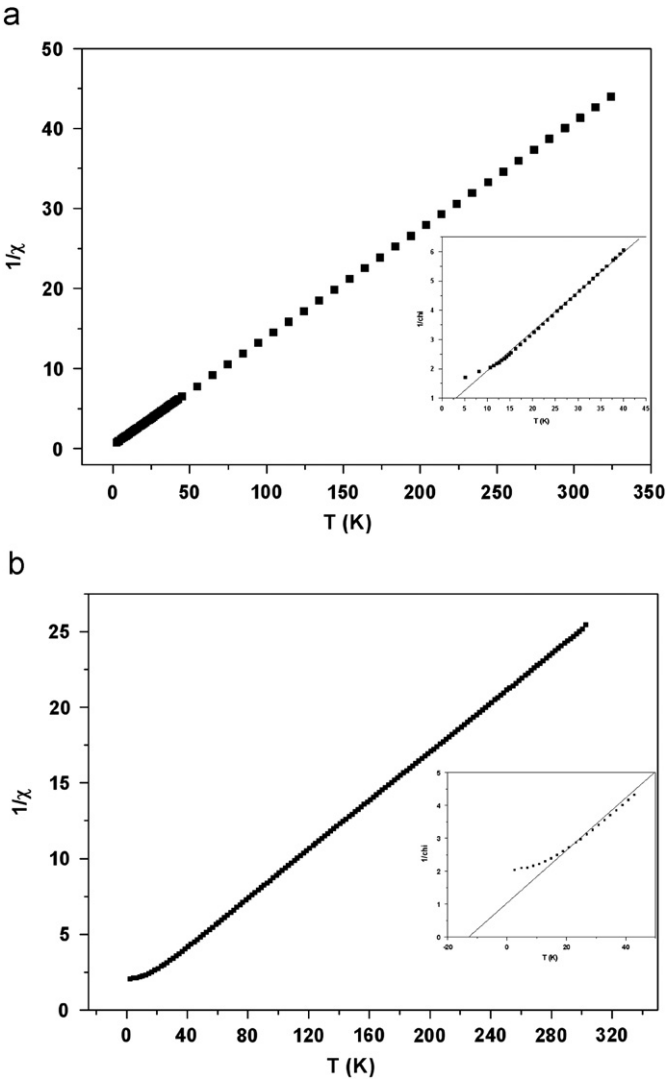

Fig. 10. A plot of inverse susceptibility as a function of temperature (a) $Gd_5Si_2BO_{13}$ (b) $Dy_5Si_2BO_{13}$.

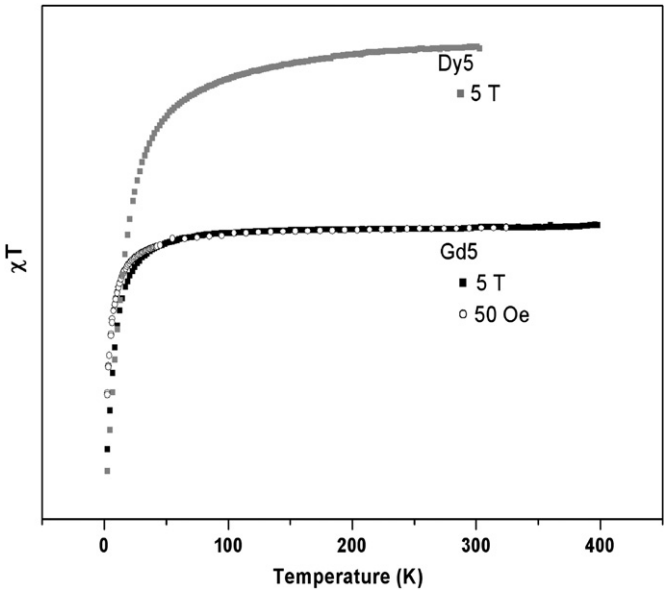

Fig. 11. A plot for susceptibility temperature product as a function of temperature.

Curie–Weiss behavior is evident below 10 and 20 K for $Gd_5Si_2BO_{13}$ and $Dy_5Si_2BO_{13}$, respectively. The χT vs. T plots are shown in Fig. 11. It is clear that antiferromagnetic interactions exist in both the compounds. However, in the presently studied compounds, both 4*f* and 6*h* sites contain rare earth ions as established from the structural and PL data. The shortest direct distance between rare earth ions is found to be between the ions present in 4*f* sites and are: Gd–Gd = 3.368 Å and Dy–Dy = 3.329 Å. In $Sr_2Nd_8(SiO_4)_6O_2$ compound with apatite structure, ferromagnetic interactions have been found when the Nd–Nd distance is more than 3.509 Å [21]. The observed distances in the present compounds are much smaller than 3.509 Å. Thus, the observed antiferromagnetic interactions in the present compounds may have origin in the short *Ln–Ln* distances.

4. Conclusion

Eu^{3+} luminescence is used as a local structural probe in $La_5Si_2BO_{13}$ with apatite related structure. PL emission studies show that Eu^{3+} occupies two different crystallographic sites La(1) and La(2). The $^5D_0$–$^7F_0$ transition of Eu^{3+} plays an important role in determining the occupancy of Eu^{3+} in different crystallographic sites. The observed two transitions for the $^5D_0$–$^7F_0$ transitions at low concentrations of Eu^{3+} indicate that Eu^{3+} occupies two different cationic sites. The increase in intensity of the emission corresponding to that of $^5D_0$–$^7F_0$ transition with increasing Eu^{3+} content reveals that the occupancy of La(2) site at 6*h* position by Eu^{3+} is more vis-a-vis the La(1) site at 4*f* position due to the existence of short La(2)–O(4) covalent bond. $Ln_5Si_2BO_{13}$ phases are isostructural with $La_5Si_2BO_{13}$. The observed antiferromagnetic interactions at low temperature in $Gd_5Si_2BO_{13}$ and $Dy_5Si_2BO_{13}$ phases can be attributed to the short *Ln–Ln* bond distances, confirmed by the structure refinement.

Acknowledgments

This work is carried out in the framework of LAFICS and the financial support from IFCPAR (Indo-French Centre for the Promotion of Advanced Research/Centre Franco-Indian Pour la Promotion de la Recherché Advance) is gratefully acknowledged. The authors acknowledge to Dr. N. Lakshminarasimhan for helpful discussions and Dr. M.V.V.M. Satyakishore for help in the Rietveld refinement.

References

[1] K. Sudarsanan, P.E. Mackie, R.A Young, Mater. Res. Bull. 7 (1972) 1331–1338.
[2] G. Blasse, J. Solid State Chem. 14 (1975) 181–184.
[3] R.G. Pappalardo, J. Walsh, R.B. Hunt Jr, J. Electrochem. Soc. 130 (1983) 2087–2096.
[4] J.P. Budin, J.C. Michel, F. Auzel, J. Appl. Phys. 50 (1979) 641–646.
[5] A.R. West, in: Solid State Chemistry and its Applications, John Wiley & Sons Ltd., Singapore, 1989.
[6] G. Blasse, B.C. Grabmaier, in: Luminescent Materials, Springer-Verlag, Berlin, 1994.
[7] G. Blasse, A. Bril, W.C. Nieuwpoort, J. Phys. Chem. Solids 27 (1966) 1587–1592.
[8] L. Boyer, B. Piriou, J. Carpena, J.L. Lacout, J. Alloys Compd. 311 (2000) 143–152.
[9] R. Jagannathan, M. Kottaisamy, J. Phys: Condens. Matter 7 (1995) 8453–8466.
[10] M. Graft, R. Reisfeld, G. Panczer, S. Shoval, B. Champagnon, G. Boulon, J. Lumin. 72-74 (1997) 572–574.
[11] J.E.H. Sansom, D. Richings, P.R. Slater, J. Solid State Chem. 139 (2001) 205–210.
[12] L.L. Reina, M.C.M. Sedeña, E.R. Losilla, A. Cabeza, M.M. Lara, S. Bruque, F.M.B. Marques, D.V. Sheptyakov, M.A.G. Aranda, Chem. Mater. 15 (2003) 2099–2108.
[13] E.H. Arbib, E. Eloudi, J.P. Chaminade, J. Darriet, Mater. Res. Bull. 35 (2000) 761–773.
[14] D. Mazza, M. Tribaudino, A. Delmastro, B. Lebech, J. Solid State Chem. 155 (2000) 389–393.
[15] J. Yuan, Z. Zhang, X. Wang, H. Chen, J. Zhao, G. Zhang, C. Shi, J. Solid State Chem. (2007) 1365–1371.
[16] Y.H. Wang, X. Guo, T. Endo, Y. Murakami, M. Ushirozawa, J. Solid State Chem. (2004) 2242–2248.
[17] M. Tukia, J. Hölsä, M. Lastusaari, J. Niittykoski, Opt. Mater. 27 (2005) 1516–1522.
[18] S. Kubota, R.L. Stanger, Y. Suzuyama, H. Yamane, M. Shimada, J. Electrochem. Soc. 149 (2002) 134–H137.
[19] B. Piriou, D. Fahmi, J. Dexpert-Ghys, A. Taitai, J.L. Lacout, J. Lumin. 39 (1987) 97–103.
[20] N. Lakshminarasimhan, U.V. Varadaraju, J. Solid State Chem. 177 (2004) 3536–3544.
[21] I. Mayer, A. Semadja, J. Solid State Chem. 43 (1982) 1–4.